Available online at www.sciencedirect.com
ScienceDirect
Progress in Natural Science 18 (2008) 931–937
Progress in Natural Science
www.elsevier.com/locate/pnsc

Computer simulation on reliability of retention index with FDG–PET and optimization of dual-time-point imaging protocol

Rui Jia [a], Jing Bai [a,*], Lingfeng Wen [b,c], Dagan Feng [b,c]

[a] *Department of Biomedical Engineering, Tsinghua University, Room B209, Building of Medical Science, Beijing 100084, China*
[b] *School of Information Technologies, University of Sydney, NSW 2006, Australia*
[c] *Department of Electronic and Information Engineering, Hong Kong Polytechnic University, Hong Kong*

Received 25 December 2007; received in revised form 9 March 2008; accepted 10 March 2008

Abstract

The inherent noise in positron emission tomography (PET) leads to the instability of quantitative indicators, which may affect the diagnostic accuracy for differentiating malignant and benign lesions in the management of lung cancer. In this paper, the reliability of retention index (RI) is systematically investigated by using computer simulation for the dual-time-point imaging protocol. The area under the receiver operating characteristic (ROC) curve is used to evaluate the optimal protocol. Results demonstrate that the reliability of RI is affected by several factors including noise level, lesion type, and imaging schedule. The RIs with small absolute values suffer from worse reliability than those larger ones. The results of ROC curves show that over delayed second scan cannot help to improve the diagnostic performance further, while an early first scan is expected. The method of optimization based on ROC analysis can be easily extended to comprise as many lesions as possible.

Keywords: Reliability; Retention index; PET (positron emission tomography); Simulation; ROC (receiver operating characteristic)

1. Introduction

In recent years, PET imaging with ^{18}F-FDG has become a mainstay for the diagnosis and management of lung cancer. However, FDG is not a tumor-specific tracer. Many clinical studies have observed that benign inflammatory or infectious lesions also show an elevated FDG uptake [1,2], similar to those of tumors, at the uptake periods. This gives rise to the false-positive diagnosis of lung cancer through visual interpretation or semi-quantitative index of standardized uptake value (SUV).

Different time activity patterns of FDG uptake and distinct net rates of FDG uptake (K_i) have been observed between malignant and benign lesions in some clinical studies [3,4], thus it is expected that the dynamic scan should be better for differentiating benign from malignant lesions than single static scan. However, the requirements of long study time and invasive sampling of plasma time activity curve (PTAC) for deriving K_i limit the clinical popularity of the dynamic scan. The alternative way to tackle the challenge is to derive the changes of two-time-point uptakes, which only requires dual-time-point imaging. Retention index (RI) has been used to derive this relative change with the potential to improve the diagnostic accuracy compared with SUV in some clinical studies [5,6].

PET imaging is regarded as a quantitative functional imaging. However, there are many factors, such as Poisson noise in radioactive decay, scatter and random coincidence, affecting the quantity of PET measurement [7]. Reliability is one important statistical feature to describe the consistency of quantitative measurement. Several clinical experiments have been carried out to evaluate the reliability of SUV and K_i [8,9], but no similar clinical research has been

* Corresponding author. Tel.: +86 13501285653; fax: +86 10 62780650.
E-mail address: deabj@tsinghua.edu.cn (J. Bai).

1002-0071/$ - see front matter © 2008 National Natural Science Foundation of China and Chinese Academy of Sciences. Published by Elsevier Limited and Science in China Press. All rights reserved.
doi:10.1016/j.pnsc.2008.03.004

done on RI. Although SUV was observed to have good reproducibility with a standard deviation around 10%, RI is calculated based on two SUVs, thus undoubtedly would suffer greater unstableness. It is unclear whether RI's reliability is related with several factors including imaging schedules, lesion type, etc., and how the reliability affects the diagnostic performance. We have done some preliminary research to investigate one fixed imaging schedule based on the kinetics of four lesion tissues [10]. In this paper, we extended the investigation on the reliability of RI with more comprehensive analysis based on more imaging schedules and the kinetics of five lesions.

Different institutions and medical imaging centers have chosen different dual-time-point scanning protocols (or sampling schedules) based on intuition and/or practical experience. This has given rise to the difficulty for a fair comparison of their protocols, and restricted the development and adoption of this effective diagnostic method. Therefore, it is necessary to develop an efficient approach to determine the optimal dual-time-point protocol for FDG–PET imaging, to help clinicians in the diagnosis of lung lesions. In this work, we investigated the performance of the area under the receiver operating characteristic (ROC) curve for evaluating dual-time-point protocols.

2. Method

2.1. Kinetic model of FDG metabolism and variance of noise for PET measurement

In this work, the classical kinetic model of FDG metabolism, which has three compartments and four parameters [11], is used to derive tissue time activity curves (TTACs) for both benign and malignant lesions. Based on this model, the relationship between the plasma time activity curve (PTAC) and TTAC complies with:

$$\begin{cases} C_i(t) = \frac{k_1}{a_2-a_1} \\ \qquad \times[(k_3+k_4-a_1)\mathrm{e}^{-a_1 t}+(a_2-k_3-k_4)\mathrm{e}^{-a_2 t}]\otimes C_P(t) \\ a_{1,2} = \frac{k_2+k_3+k_4 \mp \sqrt{(k_2+k_3+k_4)^2-4k_2k_4}}{2} \end{cases} \tag{1}$$

where $k_1 - k_4$ are the rate constants of mass exchange between the compartments, $C_i(t)$ and $C_P(t)$ represent TTAC and PTAC, respectively.

The PTAC model proposed by Feng et al. [12] is used as the input function in this investigation. The mathematical expression for this PTAC model without the delay factor is given in:

$$C_P(t) = (A_1 t - A_2 - A_3)\exp(\lambda_1 t) + A_2\exp(\lambda_2 t) + A_3\exp(\lambda_3 t) \tag{2}$$

Parameters used in Eq. (2) are as follows: $A_1 = 851.1225$ μCi/ml/min, $A_2 = 21.8798$ μCi/ml, $A_3 = 20.8113$ μCi/ml, $\lambda_1 = -4.1339\ \mathrm{min}^{-1}$, $\lambda_2 = -0.1191\ \mathrm{min}^{-1}$, $\lambda_3 = -0.0104\ \mathrm{min}^{-1}$.

Table 1 lists all the kinetic constants for lung malignant and benign lesions which are used in this study.

Due to the characteristics of PET, the measurement of PET imaging is to obtain accumulated number of detected photons averaged over the scan duration. Usually, the additive Gaussian noise is assumed to describe the noise distribution for TTAC in functional imaging as [17]:

$$\begin{cases} C(t_m) = C_o(t_m) + e(t_m) \\ C_o(t_m) = \frac{1}{\Delta t_k}\int_{t_m-\Delta t_k/2}^{t_m+\Delta t_k/2} C_i(t)\mathrm{d}t \\ \sigma^2(e(t_m)) = \frac{a\times C_o(t_m)}{\Delta t_k} \end{cases} \tag{3}$$

where t_m is the middle time of one static scan with the duration of Δt_k, $C(t_m)$ and $C_o(t_m)$ are, respectively, the measurement value and the ideal value of aggregate tissue tracer activity over Δt_k. $C_i(t)$ is defined in Eq. (1), which represents the instantaneous value of tissue tracer activity, $e(t_m)$ and $\sigma^2(e(t_m))$ are the noise term of TTAC measurement and corresponding variance over Δt_k, respectively. a is a proportional constant which determines the desired noise level, which is affected by many factors including PET imaging system, the activity contrast between the region of interest and the adjacent tissue, and reconstruction method, etc.

To investigate dual-time-point imaging schedules with long study time, we extend the above noise distribution model with the effect of decay correction included. Let $C_o(t_m)$ in Eq. (3) represents the non-decay corrected ideal tissue tracer activity over Δt_k, then the decay corrected tissue tracer activity $C_{\mathrm{dec}}(t_m)$ can be represented by $C_o(t_m)$ with the approximate equation of $C_{\mathrm{dec}}(t_m) = \exp(\lambda t_m) \times C_o(t_m)$. The noise variance of non-decay corrected measurement is also assumed to obey Eq. (3), and then the noise variance of decay corrected measurement $\sigma^2(e_{\mathrm{dec}}(t_m))$ can be estimated as follows [10,18]:

$$\begin{aligned} \sigma^2(e_{\mathrm{dec}}(t_m)) &= \sigma^2(e(t_m)\times\exp(\lambda t_m)) \\ &= \exp(2\lambda t_m)\times\sigma^2(e(t_m)) \\ &= \frac{a\times\exp(\lambda t_m)\times\exp(\lambda t_m)\times C_o(t_m)}{\Delta t_k} \\ &= \frac{a\times\exp(\lambda t_m)\times C_{\mathrm{dec}}(t_m)}{\Delta t_k} \end{aligned} \tag{4}$$

where $\lambda = \ln(2)/T_{1/2}$, $T_{1/2}$ is the half-life of Fluorine-18. For clarity, we still use $e(t_m)$ and $C_o(t_m)$ to represent the decay corrected noise variance of PET measurement and decay corrected ideal value of tissue tracer activity over Δt_k, thus Eq. (3) can be extended to Eq. (5) to incorporate the effect of decay correction

$$\begin{cases} C(t_m) = C_o(t_m) + e(t_m) \\ \sigma^2(e(t_m)) = \frac{a\times\exp(\lambda t_m)\times C_o(t_m)}{\Delta t_k} \end{cases} \tag{5}$$

Table 1
Kinetic constants for lung malignant and benign lesions

Tissue	K_1 (min^{-1})	K_2 (min^{-1})	K_3 (min^{-1})	K_4 (min^{-1})	K_i[a]
Stage III non-small-cell lung cancer [13] (M_1)	0.084	0.021	0.072	0	0.0650
Lung carcinoma [14] (M_2)	0.139	0.296	0.164	0	0.0496
Primary lung cancers [15] (M_3)	0.231	1.149	0.259	0	0.0425
Lung aspergillosis infection [16] (B_1)	0.1993	0.9778	0.2403	0.0102	0.039
Lung coccidiomycosis infection [16] (B_2)	0.1810	0.8692	0.0389	0.0007	0.0078

[a] $K_i = (K_1 * K_3)/(K_2 + K_3)$.

2.2. Computer simulation of the reliability of retention index

Retention index is a parameter for describing the relative change of the delayed SUV compared with the early SUV as follows:

$$\mathrm{RI} = \frac{\mathrm{SUV}(t_2) - \mathrm{SUV}(t_1)}{\mathrm{SUV}(t_1)} = \frac{C(t_2) - C(t_1)}{C(t_1)} \tag{6}$$

where $C(t_1)$ and $C(t_2)$ are the tissue time activities of the early and delayed scan, respectively. In this study, a particular dual-time-point imaging schedule, which comprises two scans with durations d_1 and d_2, middle times t_1 and t_2, is represented by a vector $[t_1, d_1, t_2, d_2]$. For any imaging schedule and any tissue, the ideal value of RI (RIr) is calculated through Eqs. (1) and (6), and the realistic values of RI are estimated for 10,000 times through Eqs. (5) and (6), subsequently the CV (coefficient of variance) of RI is calculated based on these 10,000 values as:

$$\mathrm{CV}(\mathrm{RI}([t_1, d_1, t_2, d_2], T_k)) = \frac{\mathrm{std}(RI_i)}{\mathrm{mean}(RI_i)}, \quad T = B \text{ or } M \tag{7}$$

where RI_i represents 10,000 simulated measurement values of RI for a specific dual-time-point imaging schedule $[t_1, d_1, t_2, d_2]$ and a specific lesion T_k, std and mean are their standard deviation and mean value, respectively. In this study, CV is used as the index to evaluate the reliability of RI.

2.3. Evaluation and optimization of dual-time-point imaging protocols

For a specific imaging schedule and a specific tissue, 10,000 measurement values of RI are compared with a given threshold for the differentiation, which classify the instance to be malignant for the values above the threshold, while to be benign for the below values. The ratio of the correct differentiation is then calculated as the diagnostic accuracy (accuracy($[t_1, d_1, t_2, d_2]$, T_k), $T = B$ or M). Based on the diagnostic accuracies of a specific imaging schedule for all five lesions, the sensitivity and specificity of a specific imaging schedule are derived in:

$$\begin{aligned}\mathrm{sensitivity}([t_1, d_1, t_2, d_2]) &= \sum_{k=1}^{3} \mathrm{accuracy}([t_1, d_1, t_2, d_2], M_k) \\ &\quad \times \mathrm{incidence}(M_k) / \sum_{k=1}^{3} \mathrm{incidence}(M_k) \\ \mathrm{specificity}([t_1, d_1, t_2, d_2]) &= \sum_{k=1}^{2} \mathrm{accuracy}([t_1, d_1, t_2, d_2], B_k) \\ &\quad \times \mathrm{incidence}(B_k) / \sum_{k=1}^{2} \mathrm{incidence}(B_k)\end{aligned} \tag{8}$$

where incidence (T_k), $T = B$ or M, as shown in Table 1 is the incidence rate of a specific lesion type, the sum of incidence rates of five lesions is 1.

ROC curve is plotted when multiple sensitivities and specificities are obtained by using multiple thresholds. Then the area under ROC curve (A_Z) is used to evaluate different dual-time-point imaging protocols. The imaging schedule with maximum A_Z is considered to be optimal.

3. Results

3.1. Reliability of RI and its effect on diagnostic performance

Fig. 1 illustrates the CV of RI at various noise levels when the imaging schedule $[55, 10, 115, 10]$ is used. As

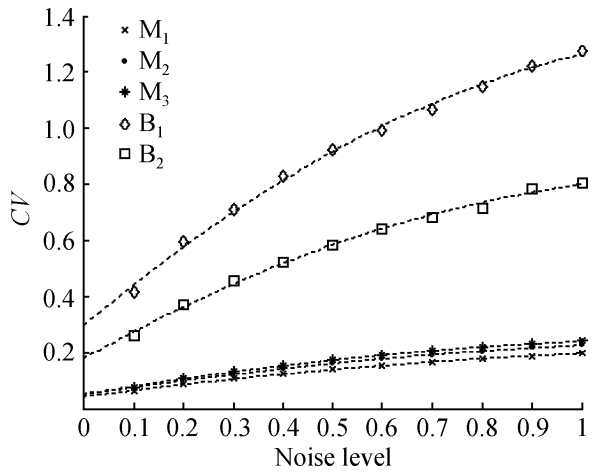

Fig. 1. CV of RI as a function of increasing noise level for the imaging schedule $[55, 10, 115, 10]$. The dashed lines are 2-order polynomial fittings of the results.

expected, CV of RI demonstrates a parabolic increasing trend as the noise level is increasing. Similar results are also observed for other imaging schedules.

Fig. 2 plots the CV of RI for M_1 as a function of varied frame durations of d_1 and d_2 for the imaging schedule [55, d_1, 175, d_2], where d_1 and d_2 are varied from 3 min to 15 min in the step of 3 min. It is observed that the reliability of RI is improved with the increased duration of either scan. Similar results are observed for other imaging schedules and studied lesions (Table 1).

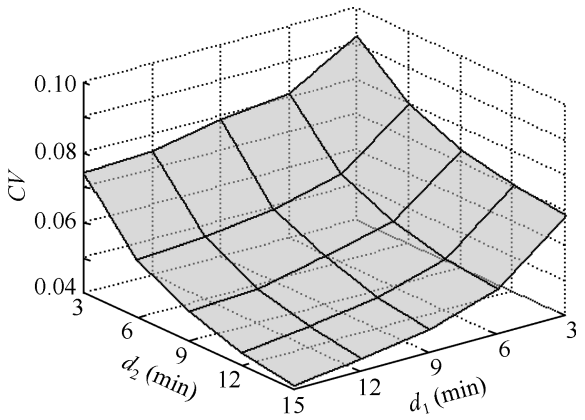

Fig. 2. CV of RI for M_1 changed with frame duration. Noise level $a = 0.1$. Imaging schedules [55, d_1, 175, d_2], where both d_1 and d_2 vary from 3 to 15 in step of 3 min.

We also observe that there is a linear relationship between CV of RI and 1/|RIr| when the duration of one scan is fixed while the middle time and duration of another scan are both fixed. Fig. 3 illustrates this linear relationship for the imaging schedules $[45, 5, t_2, 10]$, with t_2 varied from 65 to 295 in the step of 10 min, and $[t_1, 5, 150, 10]$, with t_1 varied from 10 to 120 in the step of 10 min.

Similarly, the linear relationship is also observed with different slopes and intercepts, respectively, for different situations, including lesion types, imaging schedules, noise level. Generally speaking, that a greater CV correlated with a greater 1/|RIr| indicates that low reliability will be achieved if only a small change of SUVs is obtained between two scans. It should be noticed that in some clinical researches, the threshold of 0.1 or 0 is used for differentiating malignant from benign lesions. Our analysis implies that RI may suffer from relatively worse reliability,

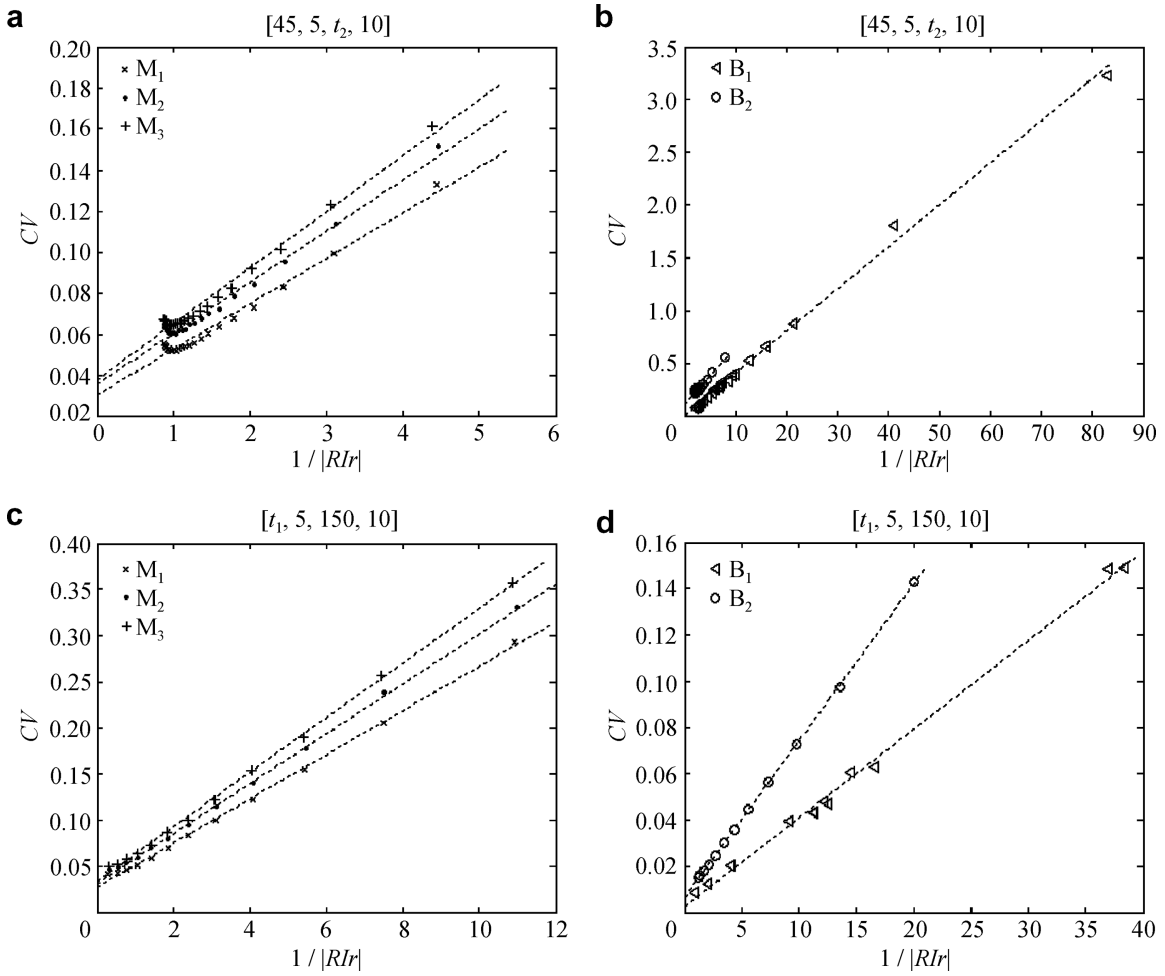

Fig. 3. Plots of the linear relationship between CV of RI and 1/|RIr| for the imaging schedules [45, 5, t_2, 10] and $[t_1, 5, 150, 10]$. t_2 varies from 65 to 295 in the step of 10 min, t_1 varies from 10 to 120 in the step of 10 min. Noise level $a = 0.1$.

affecting the diagnostic accuracy, if the absolute value of RI is too small.

For the imaging schedules $[t_1, 10,\ t_2, 10]$, where both t_1 and t_2 are varied from 5 to 295 in the step of 10 min, we plotted the results with |RIr| close to 0.1 to investigate the effect of low reliability of this index on diagnostic accuracy in Fig. 4. For malignant lesions, those schedules whose true value of RI (RIr) is within $[0.1, 0.2)$ are chosen, while the range is set to $[-0.1, 0.1)$ for benign lesions. The threshold for differentiation is set to 0.1. The simulated noise level is 0.1. Although a specific lesion should be judged correctly under its specific chosen schedules, as can be seen from Fig. 4, there are 256 points with the diagnostic accuracy lower than 0.9 over the total 413 points; the worst case is only 0.52, which indicates almost 50% chance to make wrong diagnosis for this lesion.

3.2. Optimization of dual-time-point imaging protocols

It can be known from Eq. (8) that the diagnostic sensitivity and specificity are related with the distribution of incidence rates of lesions, the derived ROC curve will vary with lesion distributions.

Regarding an even distribution of incidence rates among the studied five lesions, i.e. each lesion has an incidence rate of 20%, Fig. 5 plots the ROC curves for the imaging schedule $[30, 3, t_2, 3]$, where t_2 is varied from 50 to 100 in the step of 10 min. The noise level is 0.5. The cutoff thresholds of RI for differentiating benign and malignant lesions are varied from −1 to 1 in the step of 0.01 in the ROC analysis, thus each ROC curve has 201 points on it.

As shown in Fig. 5, when t_2 is increasing, the ROC curves move close to the left-upper corner of the graph, which means that for a fixed first scan with the middle time of 30 min and the duration of 3 min, the diagnostic performance is improved as the second scan is delayed even later.

Fig. 6 plots A_Z as a function of varied middle time for the first and the second scan. The adapted imaging schedules are $[t_1, 3, t_2, 10]$, where t_1 ranges from 30 to 80 in the step of 5 min, t_2 ranges from 60 to 180 in the step of 10 min.

As shown in Fig. 6(a), A_Z firstly keeps increasing sharply followed by the slow increase at the later stage. This implies that the proper delayed second scan can markedly improve

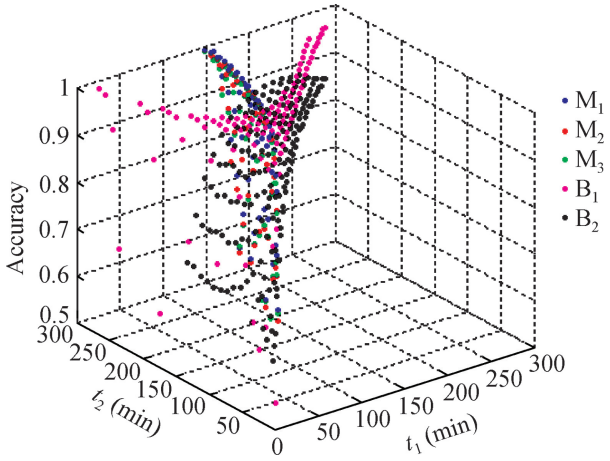

Fig. 4. Graph shows the effect of reliability of RI on its diagnostic accuracy, noise level $a = 0.1$. The numbers of schedules selected for tissues are 63 for M1, 64 for M2, 65 for M3, 103 for B1, 183 for B2.

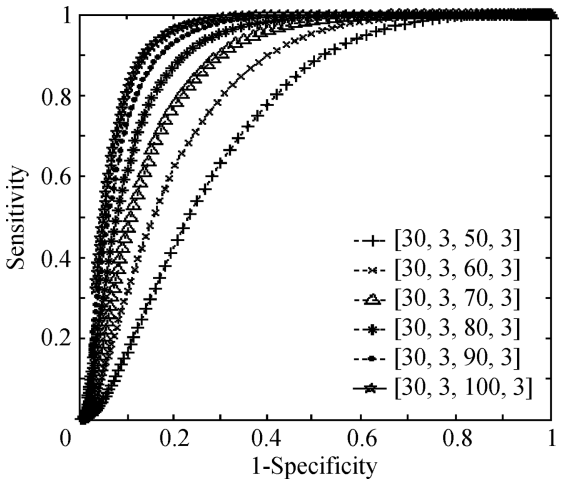

Fig. 5. ROC curves and the area under curve (A_Z) for the imaging schedules $[30, 3, t_2, 3]$, noise level $a = 0.5$.

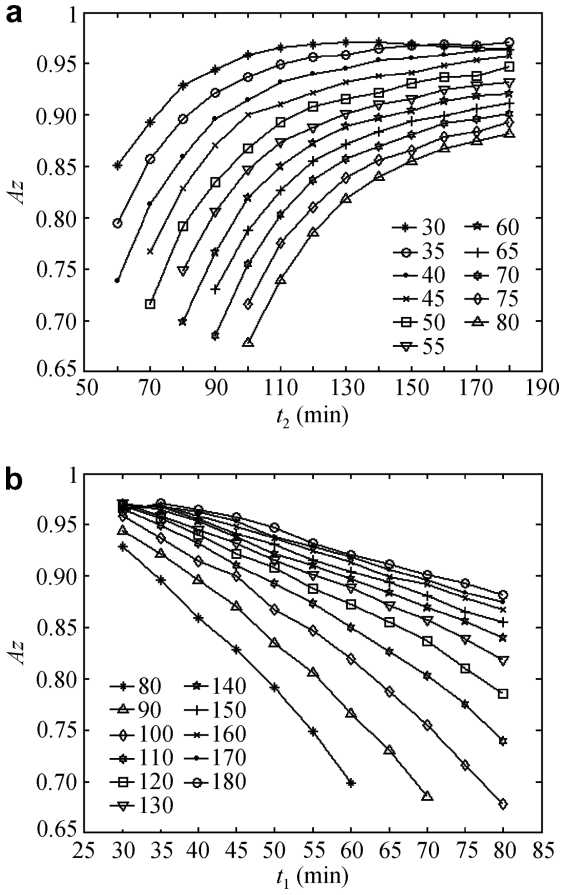

Fig. 6. The area under curve (A_Z) of imaging schedules $[t_1, 3, t_2, 10]$, noise level $a = 0.5$. (a) Each curve has the same t_1; (b) each curve has the same t_2.

the diagnostic performance of dual-time-point FDG-PET imaging, while the performance would not be improved further remarkably if the second scan is delayed too much. On the contrary, each line in Fig. 6(b) has the same t_2. It can be observed that A_Z is decreasing linearly as the first scan is delayed. This implies that the time of the first scan of dual-time-point imaging protocol is closely related with the diagnostic performance, and generally speaking, an earlier first scan is expected to improve this performance. Similar results are also observed for other incidence distributions and noise levels. For this situation of even distribution, the maximum value of A_Z is 0.9715 at the imaging schedule of [30, 3, 130, 10], which is regarded as the optimal one among all studied schedules.

4. Discussion and conclusion

Minn et al. [8] studied the reproducibility of SUV and K_i through two dynamic FDG PET examinations within 1 week for ten patients with untreated lung cancer. They found that both SUV on the basis of predicted lean body mass and influx constant of K_i provided highly reproducible indices of glucose metabolism. Weber et al. [9] examined 16 patients with altogether 50 separate tumor lesions twice by FDG PET within 10 days while no therapy was applied. They also found that SUV and K_i were highly reproducible. To our knowledge, no similar clinical research has been carried out to investigate the reproducibility of retention index. Our simulation results show that the reliability of RI is closely related with noise level, lesion type, and imaging schedule. For a specific tissue and noise level, CV of RI shows a linear relationship with $1/|\mathrm{RIr}|$ when the duration of one scan is fixed while the middle time and the duration of another scan are both fixed. For the situation that the change of SUVs is relatively small, the lesion's RI may suffer from worse reliability. This may become marked for some benign lesions. Thus the diagnosis using RI should also take the reliability into account if the absolute value of RI is relatively small.

For the five malignant/benign lesions, when the first scan is fixed and the second one gradually delayed, the area under ROC curve firstly increases sharply then followed by a slow-down tendency at the later stage, which means that the improvement of the diagnostic performance does not become obvious any more when the second scan is done later than some period. Nakamoto et al. [19] found that imaging at 3 h post injection usually was unhelpful in differentiating further between malignant lesions and benign lesions in the pancreas, which is in agreement with our simulation result in the lung. Furthermore, it is impossible to maintain many patients staying several hours in the imaging center. On the other hand, the results imply that the middle time of first scan obviously affects the diagnostic performance of dual-time-point imaging protocol, and generally an earlier first scan is expected to improve this performance. However, the very early stage of PET imaging severely suffers from Poisson noise due to considerably low activities, so it is not suggested to perform the first scan before 30 min post injection.

This study has established a frame work for objectively optimizing dual-time-point imaging protocols for the diagnosis of high FDG uptake lesions. The developed methodology can be easily extended to more lesions and different incidence rates. Further investigation will be warranted using clinical human dynamic study to evaluate the performance of the dual-time-point imaging protocols.

Acknowledgement

This work was supported by the National Natural Science Foundation of China (Grant Nos. 60331010, 60571013, and 30670577), the National Basic Research Program of China (Grant No. 2006CB705700), the Tsinghua-Yue-Yuen Medical Science Foundation, the ARC and PolyU/UGC Grants, and the Australia-China Special Fund of the Australian International Science Linkage (Grant No. CH050131).

References

[1] Bakheet SM, Saleem M, Powe J, et al. F-18 fluorodeoxyglucose chest uptake in lung inflammation and infection. Clin Nucl Med 2000;25(4):273–8.
[2] Zhuang HM, Yu JQ, Alavi A. Applications of fluorodeoxyglucose-PET imaging in the detection of infection and inflammation and other benign disorders. Radiol Clin N Am 2005;43(1):121–34.
[3] Gupta N, Gill H, Graeber G, et al. Dynamic positron emission tomography with F-18 fluorodeoxyglucose imaging in differentiation of benign from malignant lung/mediastinal lesions. Chest 1998;114(4):1105–11.
[4] Hamazawa Y, Koyama K, Okamura T, et al. Comparison of dynamic FDG-microPET study in a rabbit turpentine-induced inflammatory model and in a rabbit VX2 tumor model. Ann Nucl Med 2007;21(1):47–55.
[5] Matthies A, Hickeson M, Cuchiara A, et al. Dual time point F-18-FDG PET for the evaluation of pulmonary nodules. J Nucl Med 2002;43(7):871–5.
[6] Conrad GR, Sinha P. Narrow time-window dual-point F-18-FDG PET for the diagnosis of thoracic malignancy. Nucl Med Comm 2003;24(11):1129–37.
[7] Geng JH, Chen YM, Yin DY, et al. Noise components on positron emission tomography images. Bio-Med Mater Eng 2003;13(2):181–6.
[8] Minn H, Zasadny KR, Quint LE, et al. Lung cancer: reproducibility of quantitative measurements for evaluating 2-[F-18]-fluoro-2-deoxy-D-glucose uptake at PET. Radiology 1995;196(1):167–73.
[9] Weber WA, Ziegler SI, Thodtmann R, et al. Reproducibility of metabolic measurements in malignant tumors using FDG-PET. J Nucl Med 1999;40(11):1771–7.
[10] Jia R, Wen LF, Bai J, et al. Simulation on reliability and diagnostic accuracy of quantitative indices for FDG-PET. Tsinghua Science & Technology 2008;48(6):1049–52.
[11] Huang SC, Phelps ME, Hoffman EJ, et al. Noninvasive determination of local cerebral metabolic rate of glucose in man. Am J Physiol Endocrinol Metab 1980;238(1):E69–82.
[12] Feng D, Huang SC, Wang X. Models for computer simulation studies of input functions for tracer kinetic modeling with positron emission tomography. Int J Biomed Comput 1993;32(2):95–110.
[13] Hamberg LM, Hunter GJ, Alpert NM, et al. The dose uptake ratio as an index of glucose metabolism—useful parameter or oversimplification. J Nucl Med 1994;35(8):1308–12.

[14] Torizuka T, Zasadny KR, Recker B, et al. Untreated primary lung and breast cancers: correlation between F-18 FDG kinetic rate constants and findings of *in vitro* studies. Radiology 1998;207(3):767–74.
[15] Torizuka T, Nobezawa S, Momiki S, et al. Short dynamic FDG-PET imaging protocol for patients with lung cancer. Eur J Nucl Med 2000;27(10):1538–42.
[16] Lowe VJ, DeLong DM, Hoffman JM, et al. Optimum scanning protocol for FDG-PET evaluation of pulmonary malignancy. J Nucl Med 1995;36(5):883–7.
[17] Chen K, Huang SC, Yu DC. The effects of measurement errors in the plasma radioactivity curve on parameter-estimation in positron emission tomography. Phys Med Biol 1991;36(9):1183–200.
[18] Jia R, Eberl S, Wen L, et al. Optimal dual time point for FDG-PET in the differentiation of benign from malignant lung lesions: a simulation study. In: Annual International Conference of the IEEE Engineering in Medicine and Biology—Proceedings, 2007, pp. 4169–72.
[19] Nakamoto Y, Higashi T, Sakahara H, et al. Delayed F-18-fluoro-2-deoxy-D-glucose positron emission tomography scan for differentiation between malignant and benign lesions in the pancreas. Cancer 2000;89(12):2547–54.